



*Supplement of*

## **A phase separation inlet for droplets, ice residuals, and interstitial aerosol particles**

**Libby Koolik et al.**

*Correspondence to:* Daniel J. Cziczo ([djcziczo@purdue.edu](mailto:djcziczo@purdue.edu))

The copyright of individual parts of the supplement might differ from the article licence.

## S1 Weber Number Calculations

$N_{We}$  describes the ratio of the Bernoulli pressure caused by surrounding and opposing flow on a falling droplet to the surface tension of the droplet (Pruppacher and Klett, 1997). Droplet disruption has been estimated to occur for  $N_{We}$  significantly larger than 10 (Pruppacher and Klett, 1997). The following expression was used to solve for  $N_{We}$  and maximum droplet diameter ( $d_{max}$ ):

$$N_{We} = \frac{\rho_a d_{max} U_\infty^2}{\sigma}, \quad (1)$$

$$d_{max} = \frac{8\sigma}{C_D \rho_a U_\infty^2}, \quad (2)$$

where  $\rho_a$  refers to density of the surrounding air,  $\sigma$  is the surface tension of the droplet,  $U_\infty$  is the difference between the droplet velocity and the gas velocity, and  $C_D$  refers to the drag coefficient (Pekour and Cziczo, 2011). The droplet velocity was approximated using the following expression from Pekour and Cziczo (2011):

$$\frac{m_p v_i^2}{2} = \frac{m_p v_{i-1}^2}{2} + \Delta X \cdot F_{D_{i-1}}, \quad (3)$$

$$F_D = \frac{\pi C_D \rho_a v^2 \chi^2 d_{max}^2}{8 C_c}, \quad (4)$$

where  $C_D$  refers to the drag coefficient,  $\chi$  is the shape factor, and  $C_c$  is the slip factor.

$N_{We}$  as a function of distance along the L-PCVI was modeled for droplets varying in size from 1 to 75  $\mu\text{m}$  using SPIDER's L-PCVI IF of 50.0  $\text{L min}^{-1}$  (Fig. S1). The maximum  $N_{We}$  calculated was approximately 0.3, signifying that droplets are not expected to break up in the L-PCVI using SPIDER's flow rates.

Ice crystals and supercooled droplets that pass through the L-PCVI enter the droplet evaporation chamber, which utilizes the WBF process. The chamber is held at  $-16^\circ \text{C}$  because the difference in saturation vapor pressure between water and ice is at maximum. By the end of the chamber, the ice crystals and water droplets exist in two separate size modes (i.e., ice crystals maintain their size while droplets evaporate).

$N_{We}$  was calculated for the PCVI and found to be higher for all droplets than in the L-PCVI due to higher gas velocity (Fig. S3). Still, the maximum  $N_{We}$  for the largest droplet remained below the threshold of 10, signifying that remaining droplets should not break up before rejection. Note that the 3D printed PCVI (Fig. 1) incorporates the Kulkarni et al. (2011) gradual, conical nozzle instead of stepped inlet nozzle.

## 25 S2 L-PCVI Results of D50 vs AF-to-IF Ratio

Figure S2 represents the results of D50 as a function of the ratio AF to IF. The cut-size correlates linearly to the AF to IF ratio (correlation coefficient= 0.85).

## S3 SPIDER Operating Methodology

The SPIDER startup routine was designed to ensure there is no flow blockage by moving from the bottom to the top of the instrument (i.e., farthest downstream to initial sampling of atmosphere). The first step is to connect the critical communication lines from SPIDER to the computer via USB cables; these include an Arduino UNO, which receives data from the temperature sensors (Fig. 2); a splitter (Alicat-BB9), which transmits the flow values of each mass flow controller (MFC); and the aerosol particle and residual measurement devices. Second, the vacuum pump and pressurized air are turned on to provide flows to the MFCs. Next, the PCVI flows are turned on by setting the AF followed by the PF. This starts the flow through the chamber. The last step is to turn on the flows for the L-PCVI, again turning on AF before PF.

At each point in this process, the operator verifies via pressure measurements or achieved flow rates that no flow problems have occurred. Finally, the user turns on the low-temperature cooling bath (Proline RP 1290, Lauda-Koenigshofen) and flushes the chamber with dry, filtered air.

## S4 Droplet Evaporation Models

40 The model of droplet evaporation was based on the equation of evaporation described by Lohmann et al (2016):

$$r(t) = \sqrt{r_0^2 + 2 \left( \frac{S-1}{F_k + F_d} \right) t}, \quad (5)$$

where  $r_0$  is the initial droplet radius and  $S$  is the supersaturation.  $F_k$  and  $F_d$  are defined as.

$$F_k = \rho_w \left( \frac{L_v^2}{KR_v T^2} \right), \quad (6)$$

$$F_d = \rho_w \left( \frac{R_v T}{D_v e_{s,w}(T)} \right), \quad (7)$$

45 where  $\rho_w$  is the density of liquid water,  $L_v$  is the latent heat of vaporization,  $D_v$  is the diffusion coefficient for water vapor in air,  $e_{s,w}$  is the saturation vapor pressure of water, and  $K$  is the coefficient of thermal conductivity in air. This equation is considered valid for large droplets (larger than 5  $\mu\text{m}$ ), as it neglects the effects of solution and curvature of the droplet. When sampling from clouds, the droplets should satisfy this assumption.

The model was run with the approximate chamber dimensions for a variety of initial droplet sizes (5-50  $\mu\text{m}$ ) at different system saturations (0.25, 0.5, 0.75, and 1) (Fig. S4). In the simulation where  $S = 1$ , all of the droplets retain their original

size. In the other three simulations, the 5 and 12.5  $\mu\text{m}$  droplets fully evaporate by the end of the chamber. The 25  $\mu\text{m}$  droplet evaporates fully when supersaturation is equal to or lower than 0.5.

### **S5 Bubbler Size Distribution for PCVI Verification Test**

55 A bubble burst generator (“bubbler”) was used to test the performance of the 3D printed PCVI. Figure S5 shows the number concentration of particles generated by the bubbler over a three-minute period when operated with a 0.1  $\text{g L}^{-1}$  solution of ammonium sulfate. The size distribution was measured at a one-second resolution over the course of three minutes of continuous operation.

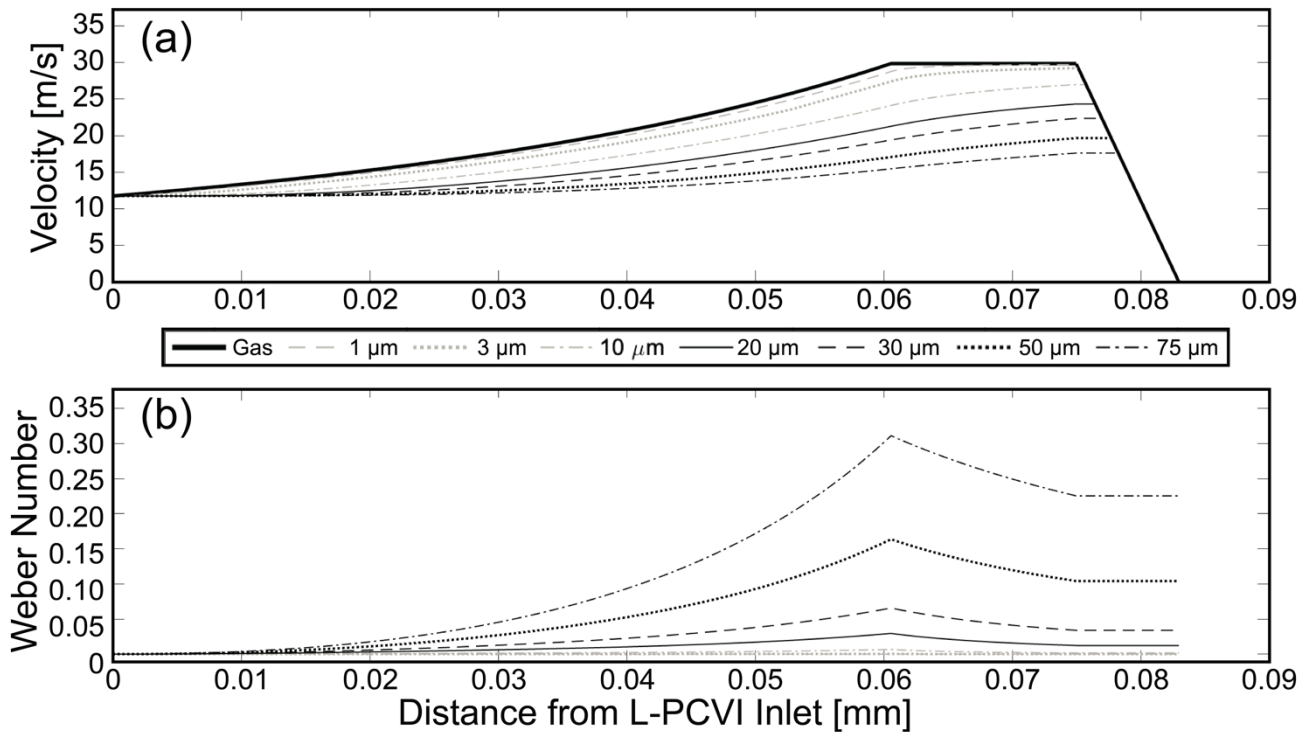
### **S6 Additional PCVI Verification Test**

60 An additional PCVI verification test was performed to characterize the rejected particles in the PF. A polydisperse particle flow from the laboratory air was used and the OPS was connected to the SF of the PCVI. Measurements at 1-second resolution were made while the PCVI flows were off to capture the distribution of particles in the input flow (Fig. S6a). Next, the OPS was disconnected from the SF and reconnected to the PF and PCVI flows were turned on (PF set to 8.0  $\text{L min}^{-1}$  and AF set to 2.5  $\text{L min}^{-1}$ ) to measure the rejected particles (Fig. S6b). Finally, the OPS was reconnected to the SF, and measurement were repeated (Fig. S6c). A comparison of Figures S6a and S6b was performed to show the PCVI was  
65 functioning correctly. In a functional PCVI, the small particles should be rejected (and pumped away in the PF), so there should be a comparable number of particles in the small bins of the SF when the PCVI flows are off to the number of particles in the small bins of the PF when the PCVI flows are on. The concentrations of particles in the three smallest bins from the operational PCVI’s PF (Fig. S6b) are within 15% of those recorded when the PCVI flows were off and the OPS was attached in the SF region (Fig. S6a). In the bins closest to the expected D50, the concentrations of larger particles in the  
70 PCVI’s PF (Fig. S6b) are much smaller (50%) than the concentrations in the SF when the PCVI flows are off (Fig. S6a). It is expected that the concentrations of particles in the PF larger than the theoretical D50 will be significantly smaller than their counterparts in the SF sample because these larger particles are transmitting through the SF of the PCVI with flows on and not being pumped away in the PF.

Additionally, Figure S6d shows the same data as Figure S6a, but with the same scaling as Figure S6c. When the PCVI flows are off (Fig. S6d), there are large numbers of small particles that are not seen in the SF when the PCVI flows are on (Fig. S6c).

## References

- 80 Kulkarni, G., Pekour, M., Afchine, A., Murphy, D. M., and Cziczo, D. J.: Comparison of experimental and numerical studies of the performance characteristics of a pumped counterflow virtual impactor, *Aerosol Sci. Tech.*, 45, 382–392, <https://doi.org/10.1080/02786826.2010.539291>, 2011.
- Lohmann, U., Lüönd, F., and Mahrt, F. (Eds.): *An Introduction to Clouds: From the Microscale to Climate*, Cambridge University Press, Cambridge, England, 2016.
- Pekour, M. S. and Cziczo, D. J.: Wake capture, particle breakup, and other artifacts associated with counterflow virtual impaction, *Aerosol Sci. Tech.*, 45, 758–764, <https://doi.org/10.1080/02786826.2011.558942>, 2011.
- 85 Pruppacher, H. R. and Klett, J. D.: *Microphysics of Clouds and Precipitation*, 2nd ed., Springer Netherlands, Dordrecht, Netherlands, 1997..



90 Figure S1: (a) Velocity calculated for droplet sizes and gas shown as a function of distance from the L-PCVI inlet. (b) The corresponding Weber number calculated along the L-PCVI inlet.

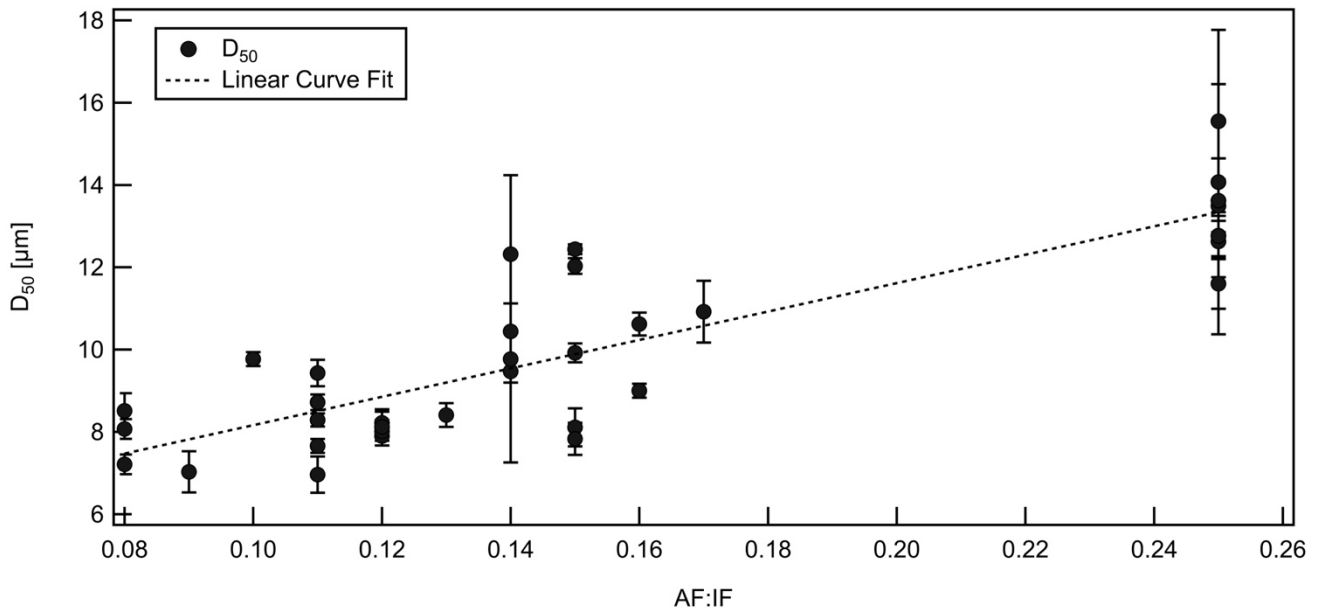


Figure S2: D50 as function of AF to IF ratio of the L-PCVI. The dashed line represents a linear curve fit (correlation coefficient=0.85). The representative error due to D50 uncertainty is shown. Uncertainty in flow rate ratio is less than the width of the data points.

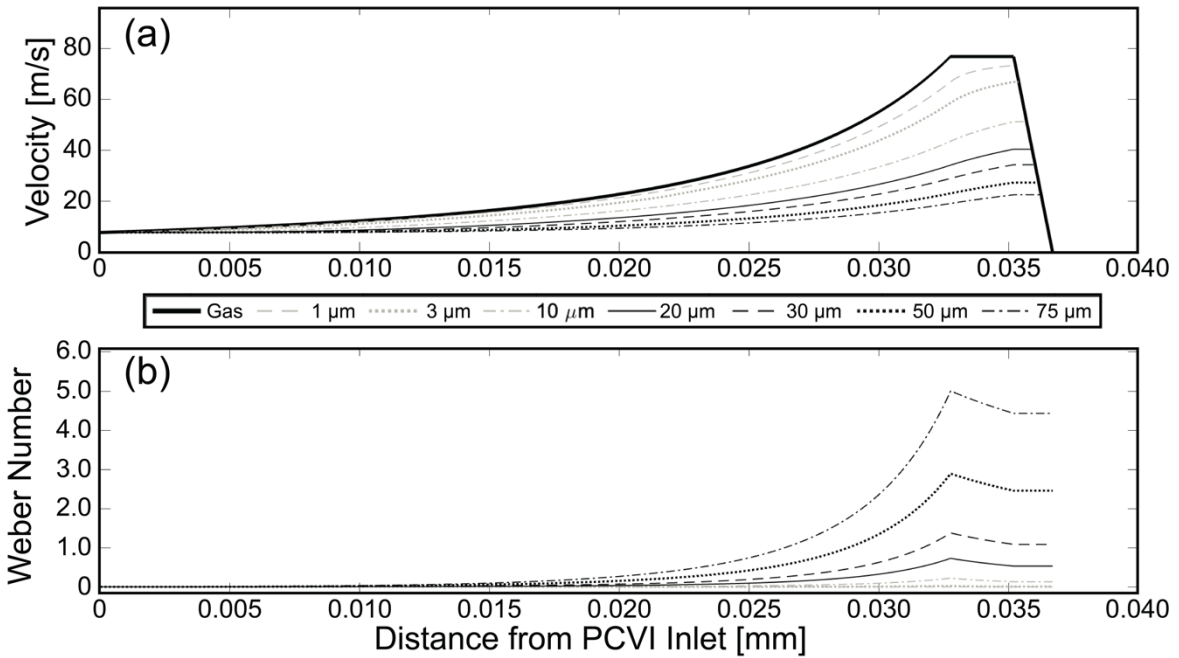
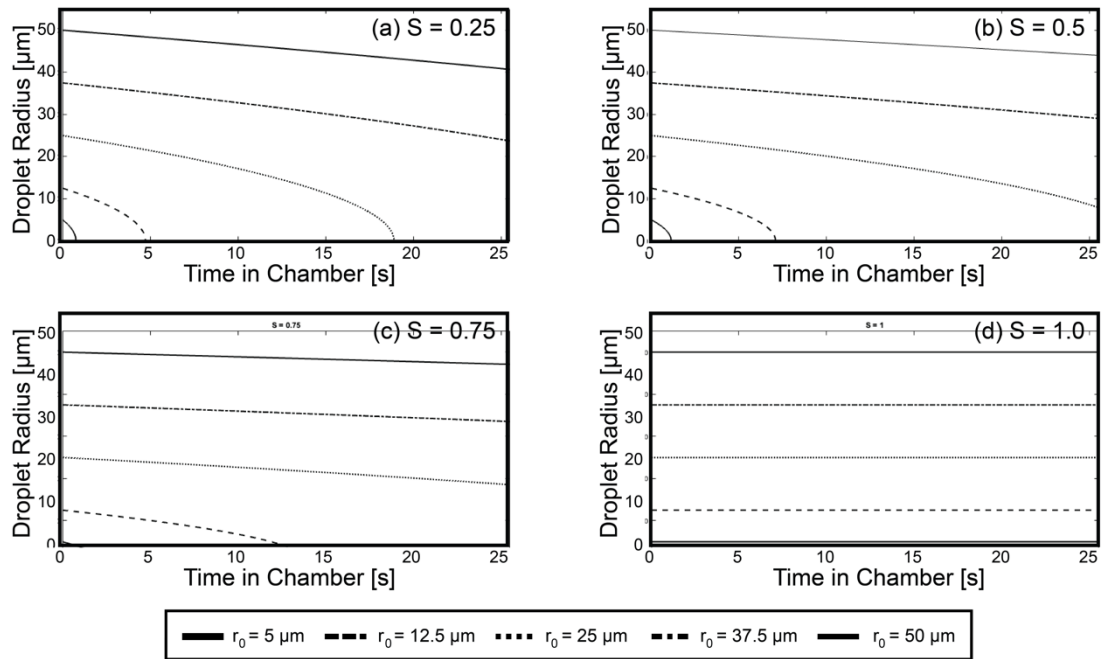
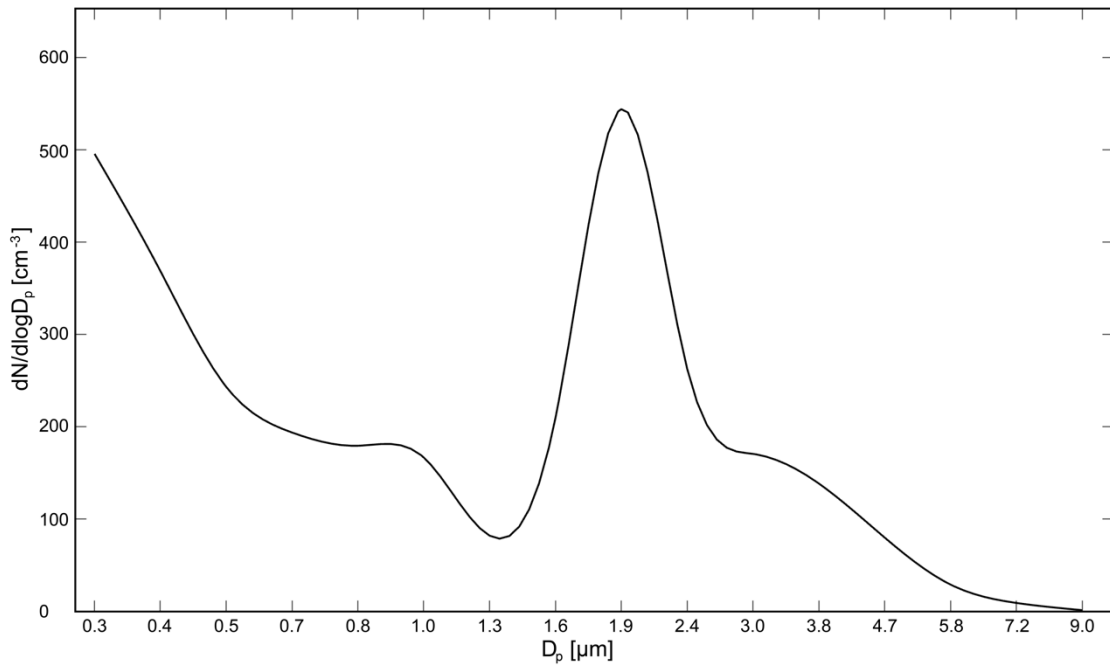


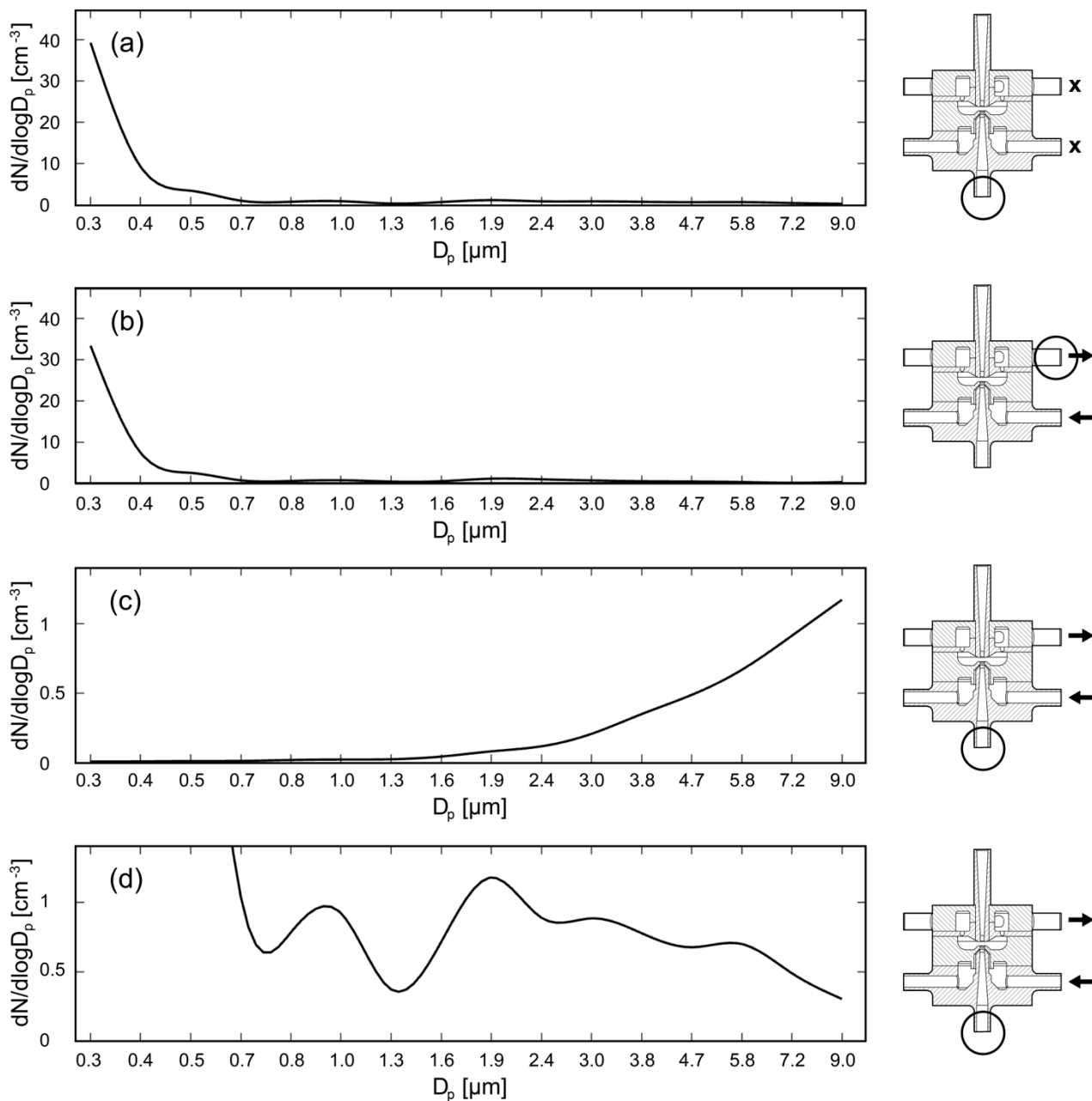
Figure S3: (a) Velocity calculated for droplet sizes and gas shown as a function of distance from the PCVI inlet. (b) The corresponding Weber number calculated along the PCVI inlet.



100 **Figure S4: Droplet size, as a function of time (i.e., evaporation time) for five initial droplet sizes relevant to SPIDER for saturation ratios of (a) 0.25, (b) 0.5, (c) 0.75, and (d) 1.0.**



**Figure S5: Number concentration as a function of particle diameter used for the first PCVI verification test. Particles are created by a bubble burst generator from a 0.1 g/L ammonium sulfate solution.**



105 **Figure S6: Number concentration as a function of particle diameter for three PCVI verification tests. (a) A control experiment with the PCVI flows turned off with the OPS in the SF. (b) The aerosol particle concentration for sizes below the PCVI D50 with**

110 the PCVI flows turned on with the OPS in the PF. (c) The PCVI flows turned on with the OPS in the SF. (d) Panel (a) is reproduced with the same y-axis as (c) for comparison. The circled region on the PCVI drawing to the right shows from which flow channel the measurement is being taken and the arrows show the direction of the flow. An “x” represents no flow. Note that the PCVI is symmetric, however for simplicity, flows are only shown on the right-hand side.